Ordered Mesoporous Metal–Phenolic Network Particles

Zhixing Lin,[†] Jiajing Zhou,[†] Christina Cortez-Jugo,[†] Yiyuan Han,[†] Yutian Ma,[†] Shuaijun Pan,[†] Eric Hanssen,[‡] Joseph J. Richardson,[†] and Frank Caruso[†,*]

[†]ARC Centre of Excellence in Convergent Bio-Nano Science and Technology, and the Department of Chemical Engineering, The University of Melbourne, Parkville, Victoria 3010, Australia.

[‡]Advanced Microscopy Facility, Bio21 Molecular Science and Biotechnology Institute, The University of Melbourne, Parkville, Victoria 3010, Australia

ABSTRACT: Mesoporous metal–organic networks have attracted widespread interest owing to their potential applications in diverse fields including gas storage, separations, catalysis, and drug delivery. Despite recent advances, the synthesis of metal–organic networks with large and ordered mesochannels (>20 nm), which are important for loading, separating, and releasing macromolecules, remains a challenge. Herein, we report a templating strategy using sacrificial double cubic network polymer cubosomes ($Im\bar{3}m$) to synthesize ordered mesoporous metal–phenolic particles (meso-MPN particles) with a large pore (~40 nm) single cubic network ($Pm\bar{3}m$). We demonstrate that the large pore network and the phenolic groups in the meso-MPN particles enable high loadings of various proteins (e.g., horseradish peroxidase (HRP), bovine hemoglobin, immunoglobulin G, and glucose oxidase (GOx)), which have different shapes, charges, and sizes (i.e., molecular weights spanning 44–160 kDa). For example, GOx loading in the meso-MPN particles was 362 mg g^{-1}, which is ~6-fold higher than the amount loaded in commercially available SiO_2 particles with an average pore size of 50 nm. Furthermore, we show that HRP, when loaded in the meso-MPN particles (486 mg g^{-1}), retained ~82% activity of free HRP in solution and can be recycled at least 5 times with a minimal (~13%) decrease in HRP activity, which exceeds HRP performance in 50-nm pore SiO_2 particles (~36% retained activity and ~30% activity loss when recycled 5 times). Considering the wide selection of naturally abundant polyphenols (>8000 species) and metal ions available, the present cubosome-enabled strategy is expected to provide new avenues for designing a range of meso-MPN particles for various applications.

INTRODUCTION

Porous materials are of widespread scientific and industrial interest and find applications in fields including catalysis and drug delivery.[1,2] Topological features, such as pore size and pore connectivity, play a central role in the design of porous materials, as they not only modulate the efficiency of mass transport, but also can screen and capture targets of interest.[3-5] Notably, the presence of large ordered mesopores, particularly those larger than 20 nm, can reduce the diffusion barrier of small molecules, functional biomacromolecules, and nanoparticles into the particles.[6,7] As a class of porous material, metal–organic networks have attracted considerable attention owing to their tunable porous structure and unique physicochemical properties originating from their constituent metal and organic building blocks.[8,9] However, the porosity within metal–organic networks is generally restricted to the microporous regime, which limits their application in various fields (e.g., protein and gene delivery). To this end, efforts have been made to generate mesoporosity within metal–organic networks via the use of extendable ligands,[10] mixed ligands,[11] and etching.[12] These approaches generally result in irregular pore architectures and/or limited pore size expansion. Templating methods have emerged as an alternative means to generate regular mesopores, where the porosity generally stems from the ordered assembly of the metal–organic networks intergrown throughout the template.[13-15] However, significant challenges remain in templating mesoporous metal–organic networks, for instance, achieving adequate interaction between the mesopore-generating template and the metal–organic replicate, and maintaining the stability of the replicated metal–organic network during template removal. Polymer cubosomes, arising from the inverse bicontinuous mesophase of block copolymers, have been reported with ordered mesopores and selective solubility.[16-21] A recent study confirmed the feasibility of using cubosomes as templates for constructing replica inorganic (SiO_2 and TiO_2) particles;[22] however, there still remains a need to establish cubosome synthesis routes to enable their use to template more complex materials, such as metal–organic systems.

Recently, our group introduced metal–phenolic networks (MPNs), a class of naturally derived low-toxicity and stimulus-responsive metal–organic networks, which can replicate diverse templates with high fidelity using the coordination between metal ions and phenolic ligands.[23-26] MPNs have been applied in various fields including bioimaging,[24] drug delivery,[27] and heavy metal

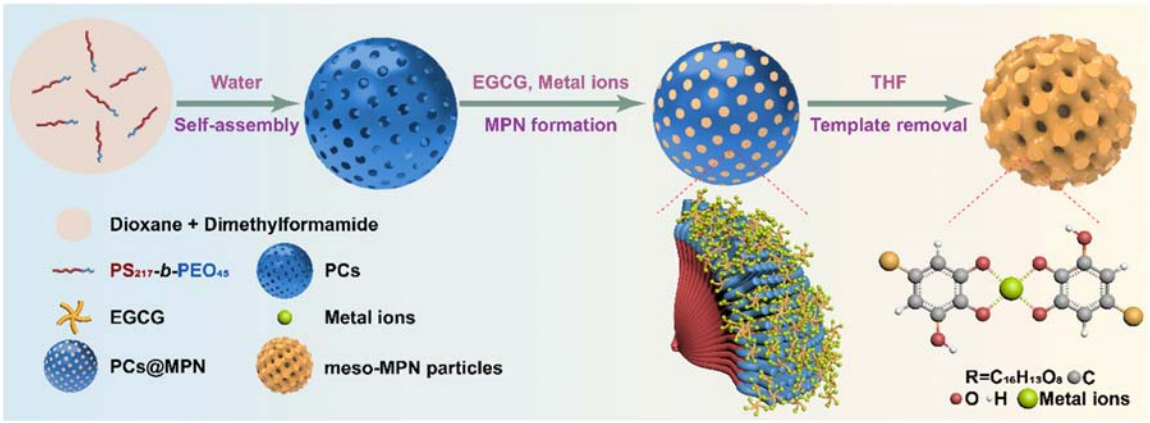

Scheme 1. Schematic of the preparation of the meso-MPN particles using PCs as templates.

extraction.[28] In addition, MPNs are stable in a wide range of solvents, making them suitable for the design of mesoporous metal–organic networks. Herein, we report a templating strategy for fabricating ordered mesoporous metal–phenolic network particles (meso-MPN particles) with a single cubic network (Scheme 1, Figure S1). Inspired by the sophisticated self-assembly of natural systems (e.g., ordered smooth endoplasmic reticulum),[29] we first assembled polymer cubosomes (PCs) from linear polystyrene-*block*-poly(ethylene oxide) (PS-*b*-PEO) and then used these PCs as templates for the synthesis of the meso-MPN particles. The PCs possess bicontinuous triply periodic minimal surface structures,[30] in which two non-intersecting large water-channel networks are weaved in a long-range cubic crystalline order. The meso-MPN particles with single networks ($Pm\bar{3}m$) were then replicated by the in situ formation of MPNs and subsequent dissolution of the PC templates by tetrahydrofuran (THF). Different phenolics (e.g., (−)-epigallocatechin gallate (EGCG) and gallic acid)) and various metal ions (Fe^{3+}, Cu^{2+}, and Zr^{4+}) were used to design different types of meso-MPN particles. We examine the ability and capacity of the meso-MPN particles as supports for loading diverse biomacromolecules and as recyclable bioreactors.

RESULTS AND DISCUSSION

The cubosomes were assembled from simple and easy-to-synthesize linear PS-*b*-PEO diblock copolymers, thereby affording a simple fabrication process and potentially extending the practical applications of the meso-MPN particles. Similar to liposomes or other surfactant assemblies, the structure of the polymer assemblies is mainly determined by a packing parameter p.[16,31,32] Therefore, a long hydrophobic block and a mixed solvent were selected to ensure a suitable p value ($p > 1$) for the formation of cubosomes. PS_{217}-*b*-PEO_{45} with a well-defined block length and narrow molecular weight distribution was synthesized via atom transfer radical polymerization (Figures S2–S4). PCs with a double primitive cubic network were subsequently self-assembled by a cosolvent method using water and a dioxane/dimethylformamide mixture.[16] Importantly, the PCs were stable in aqueous solution and readily dissolved in THF, and therefore could serve as templates for metal–organic materials that are stable in organic solvents.

The morphology of the PCs was examined prior to MPN templating (Figure 1a–c). Scanning electron microscopy (SEM) showed the near-spherical morphology of the particles with an average diameter of 2.4 ± 0.6 μm (Figures 1a, S5a) and uniform pores with a diameter of ~15 nm distributed tetragonally on the surface of the PCs (Figures 1b, S6). Transmission electron microscopy (TEM) revealed bicontinuous internal structures, with a typical [100] direction of $Im\bar{3}m$ cubic lattice (Figure 1c). The internal structure of the PCs was further investigated using synchrotron small-angle X-ray scattering (SAXS). The SAXS pattern of the PCs (Figure S7a) displayed three characteristic peaks with a scattering vector (q^2) ratio of 2:4:6, corresponding to the [110], [200], and [211] reflections of the $Im\bar{3}m$ cubic structure.[33] Cross-sectional SEM images of fractured PCs further confirmed that the internal bicontinuous porous structure was maintained along the [110] directions of the primitive cubic surface (Figure S7b), highlighting the potential of the PCs for templating ordered MPNs.

The meso-MPN particles were obtained by the infusion of small phenolic ligands (i.e., EGCG) into the pores of the PCs and subsequent in situ coordination with Fe^{3+}, followed by etching of the PC templates in THF. The template suspension changed from milky white to blue–black upon formation of the MPN coating on the PCs (Figure S8). The average diameter of the MPN-coated PCs (before template removal), i.e., PCs@MPN particles (2.4 ± 0.7 μm), was similar to that of the PCs, while the pores on the surface of the PCs@MPN particles appeared to be significantly blocked (Figure 1d,e). However, TEM analysis of PCs@MPN (Figure 1f) revealed an interconnected pore structure, thus indicating that only one set of channels was open to the surroundings and therefore the channels were filled by the MPNs.[22,34] Removal of the PC templates with THF led to the formation of ordered meso-MPN particles (Figure 1g–i). SEM analysis demonstrated uniform tetragonally distributed pores on the surface of the meso-MPN particles and pore sizes of ~40 nm (the solid walls of the PC templates become the pores of the replica particles) (Figure 1h). High-angle annular dark-field (HAADF) and energy-dispersive X-ray spectroscopy (EDX) mapping results reveal the presence of elements C, O, and Fe that were uniformly distributed throughout the meso-MPN

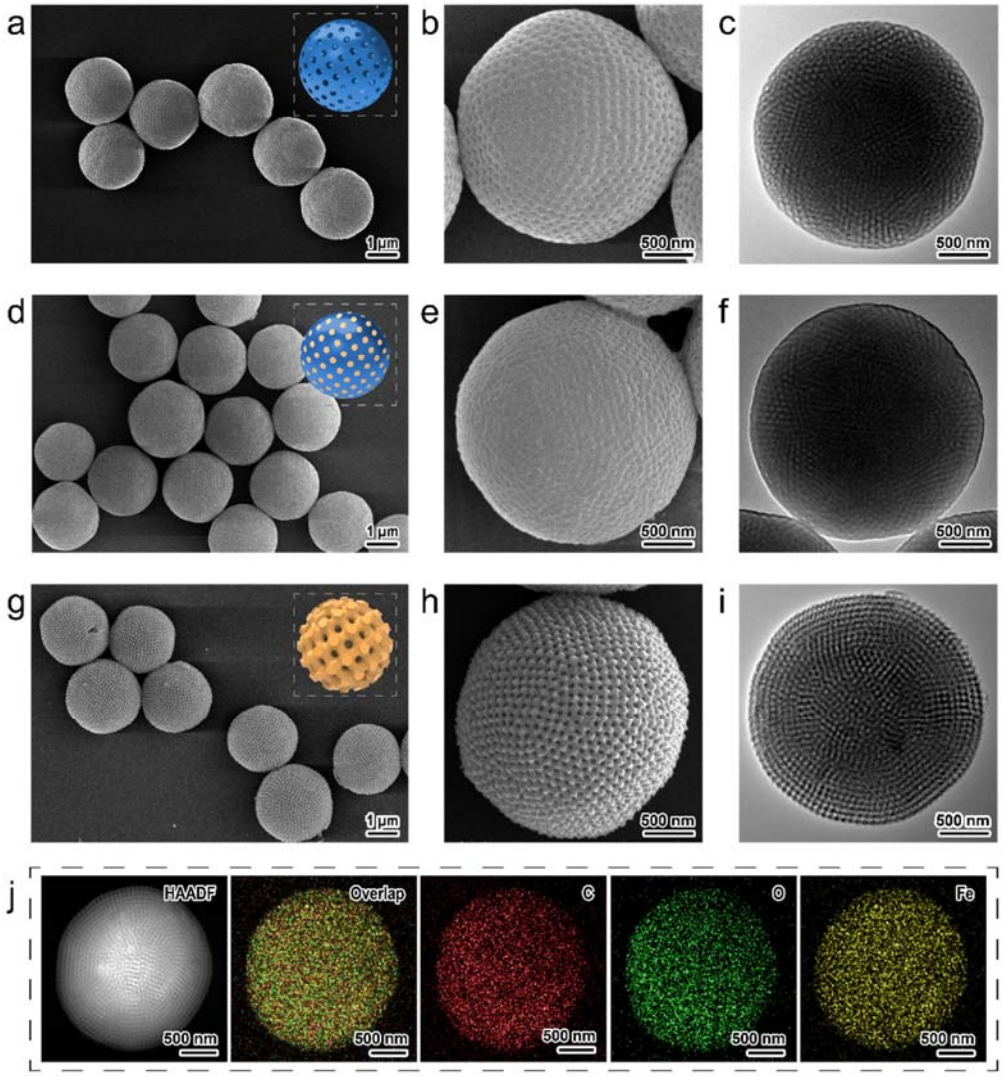

Figure 1. Representative SEM and TEM images of the (a–c) PCs, (d–f) PCs@MPN (MPN-coated PCs before template removal), and (g–i) meso-MPN particles. (j) High-angle annular dark-field (HAADF) and energy-dispersive X-ray spectroscopy elemental mapping of the meso-MPN particles.

particles, confirming the metal–organic nature of the particles (Figure 1j). Notably, no coordination cluster aggregates were observed on the surface of the meso-MPN particles.

TEM further revealed that a bicontinuous porous structure was present in the meso-MPN particles, along with the typical [100] direction of the $Pm\bar{3}m$ cubic lattice (Figure 1i). The SAXS pattern of the meso-MPN particles displayed three characteristic peaks with a q^2 ratio of 1:2:3, corresponding to the [100], [110], and [111] reflections of the $Pm\bar{3}m$ cubic structure (Figure S9).[35] The average unit cell parameter of the meso-MPN particles was 60 nm, almost identical to that of the PCs (62 nm), suggesting a conformal replica. SEM and TEM images of fractured meso-MPN particles showed the typical structure of the $Pm\bar{3}m$ cubic network with six-fold junctions from the [100] direction (Figure 2a–c), which originates from the primitive cubic lattice of the PCs. Electron tomography and computer-generated three-dimensional (3D) visualization of an internal section of the meso-MPN particles revealed the cubic mesophases of the meso-MPN particles (Figure 2d). These results indicate that the meso-MPN particles possess a $Pm\bar{3}m$ single cubic network rather than a double network structure, suggesting that the MPNs only filled/coated one set of pores in the PCs.[36]

Various characterization methods were used to confirm that the meso-MPN particles were composed of MPNs. Fourier transform infrared (FTIR) spectroscopy revealed that the carbonyl group (C=O) stretching of EGCG shifted from 1689 to 1651 cm^{-1} in PCs@MPN, which indicates strong hydrogen bonding between the PCs and EGCG. In addition, in the FTIR spectrum of the meso-MPN particles, the broadening of the absorption bands at 3349 and 3471 cm^{-1} (corresponding to HO–C stretching), which were originally distinct in the FTIR spectrum of EGCG, suggests the formation of coordination bonds between the phenolic groups and metal ions (Figure 2e). The UV–vis absorption

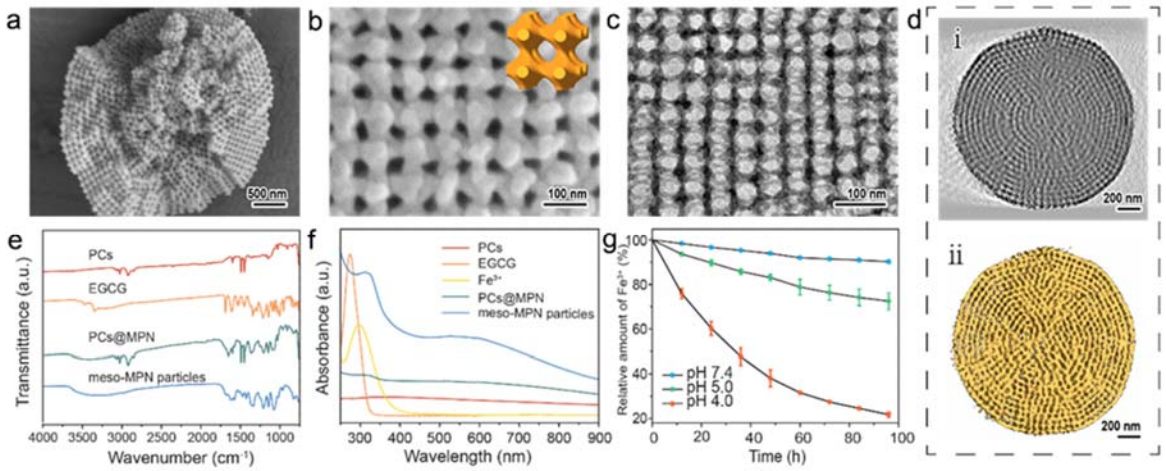

Figure 2. Structural analysis of the meso-MPN particles. (a, b) SEM and (c) TEM images of a fractured meso-MPN particle. (d) Representative internal slice of a meso-MPN particle characterized by (i) electron tomogram and (ii) computer-generated 3D visualization. (e) Fourier transform infrared spectra of the PCs, EGCG, PCs@MPN, and meso-MPN particles. (f) UV–vis absorption spectra of the PCs, EGCG, Fe^{3+}, PCs@MPN, and meso-MPN particles. (g) pH-Dependent disassembly kinetics of the Fe^{3+}-EGCG meso-MPN particles at different pH.

spectra of the meso-MPN particles showed a characteristic ligand-to-metal charge transfer (LMCT) band at ~565 nm,[37] which is absent in the spectrum of PCs or EGCG (Figure 2f). The presence of the LMCT band suggests that the meso-MPN particles are composed of bis- and tris-state MPN complexes, where the bis-state is dominant. The peak at ~712.3 eV in the X-ray photoelectron spectroscopy survey spectrum of the meso-MPN particles further confirmed the presence of Fe^{3+} in the particles (Figure S10). The MPN component of the meso-MPN particles are amorphous, as confirmed by X-ray diffraction (Figure S11). Of special interest is the versatility of this templating strategy, as we demonstrate for the preparation of various MPNs containing different metal ions (e.g., Cu^{2+}, Zr^{4+}) and polyphenols (e.g., gallic acid) (Figures S12–S15). In addition, the meso-MPN particles exhibited pH-responsive disassembly owing to the dynamic coordination between the phenolics (EGCG) and metal ions (Fe^{3+}, Figure 2g, Figure S16). At pH 7.4, 10% of the meso-MPN particles disassembled after 96 h, whereas approximately 80% of the meso-MPN particles disassembled at pH 4.0 after 96 h.

Porous particles are promising candidates for various applications including drug delivery and catalysis as they can load and release high quantities of functional macromolecules,[1] and our interest in these systems stems from our work on the encapsulation and release of proteins/therapeutics for localized delivery applications.[38] We therefore examined the accessibility of the pores within the meso-MPN particles using a range of proteins with different size, shape, and surface charge. Loading of the different cargos was conducted in phosphate buffer (pH 6). Regardless of their physicochemical features, all the proteins were successfully loaded into the meso-MPN particles. We were also able to load DNA and inorganic nanoparticles into the meso-MPN particles (Figure S17). To further investigate the protein loading profile of the meso-MPN particles, their loading was compared with that of different carriers (e.g., PCs and commercial SiO_2 microparticles with average pore sizes of 8, 20, and 50 nm; Figure S18) using model proteins with different molecular weights (Figure 3a, Table S1), including horseradish peroxidase (HRP, 44 kDa), bovine hemoglobin (BHb, 65 kDa), immunoglobulin G (IgG, 153 kDa), and glucose oxidase (GOx, 160 kDa). The PCs exhibited negligible protein loading mainly due to the antifouling properties of the PEO corona on the surface of the cubosomes. In contrast, the meso-MPN particles exhibited superior loading capacity across the whole range of proteins studied, which is attributed to the high affinity that phenolics exhibit for nearly any protein via hydrogen bonding, electrostatics, and/or hydrophobic interactions.[39-41] The meso-MPN particles also demonstrated a significantly higher loading capacity for high molecular weight proteins than the SiO_2 particles. For example, the loading amount of HRP in the meso-MPN particles was 486 mg g^{-1}, which is ~3- and ~5-fold higher than the amounts loaded in the SiO_2 particles with average pore sizes of 8 and 50 nm, respectively. HRP has a net positive charge at physiological pH and therefore could potentially electrostatically interact with the negatively charged surfaces of both SiO_2 and the meso-MPN particles. We therefore also examined the loading of a protein with a similar negative charge to the particles, and the loading of GOx in the meso-MPN particles was 362 mg g^{-1}, which is ~20- and ~6-fold higher than the amounts loaded into the SiO_2 particles with average pore sizes of 8 and 50 nm, respectively. This suggested that the high loading capacity of the meso-MPN particles across the various molecular weights of proteins can be attributed to their unique chemical nature and bicontinuous ordered porous structure. Loading throughout the meso-MPN particles was confirmed from the uniform distribution of fluorescence observed in confocal laser scanning microscopy (CLSM) images. Figure 3b shows representative CLSM images of fluorescein isothiocyanate-labeled HRP (FITC-HRP)-loaded meso-MPN particles.

The meso-MPN particles were subsequently examined as an enzyme-integrated bioreactor, and the activity of the loaded HRP was evaluated by assessing the enzymatic oxidation of amplex red in the presence of H_2O_2.[42,43]

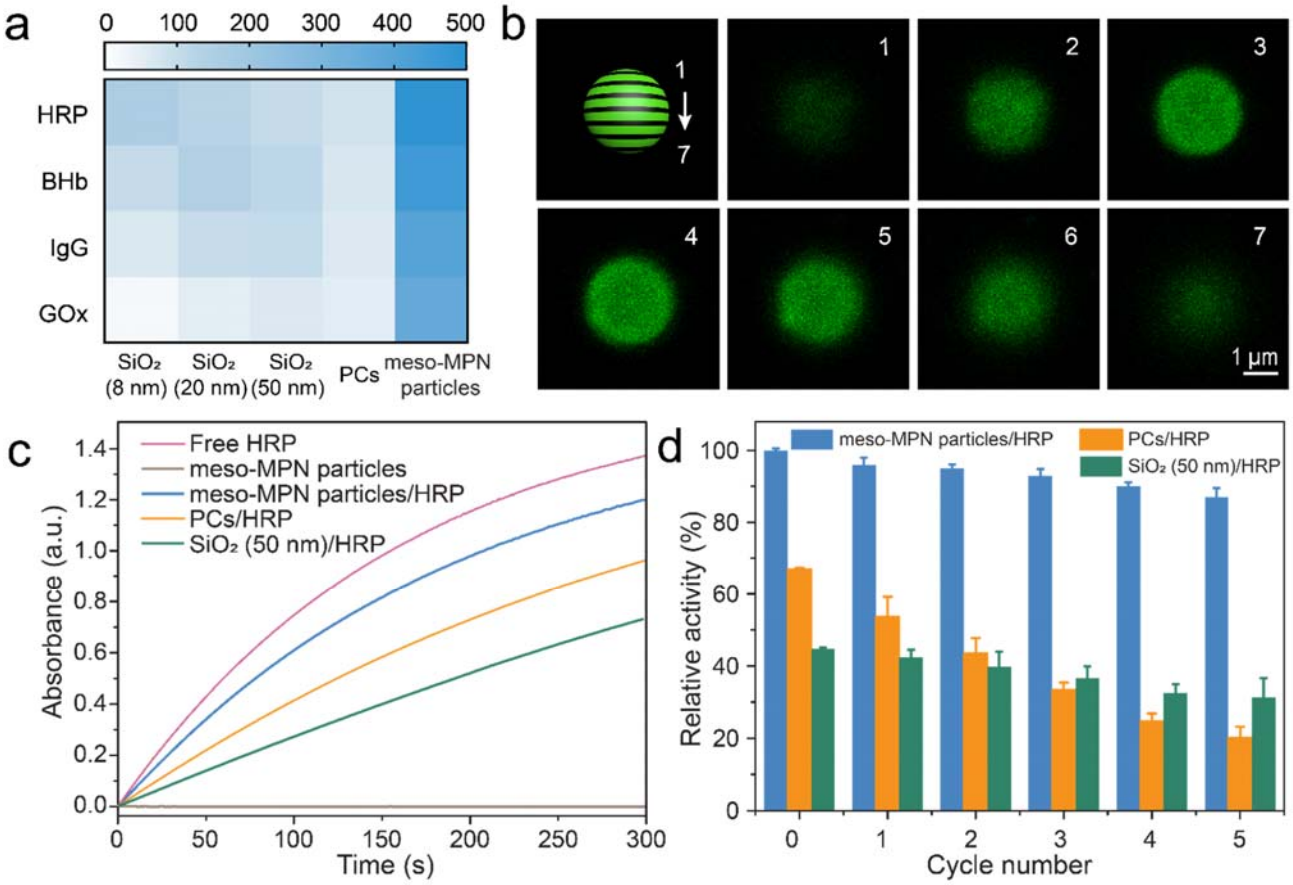

Figure 3. (a) Protein loading amount (mg g^{-1}) in the meso-MPN particles, PCs, and SiO_2 with different pore sizes. Protein concentration used for loading was 1 mg mL^{-1}. (b) Cross-sectional *z*-slice CLSM images of a meso-MPN particle loaded with FITC-HRP from the top (1) to the base (7) of the particle. (c) Time-course plots of the absorbance of amplex red oxidized by free HRP, meso-MPN particles, meso-MPN particles/HRP, PCs/HRP, SiO_2 (50 nm)/HRP in the presence of H_2O_2. (d) Recyclability of the meso-MPN particles/HRP, PCs/HRP, SiO_2 (50 nm)/HRP, as measured from the relative activity of the loaded HRP after each assay cycle versus the first cycle of the meso-MPN particles. The results are shown as means ± standard deviation ($N = 3$).

Throughout the course of the reaction, the HRP-loaded meso-MPN particles (meso-MPN particles/HRP) maintained a high reaction rate ($V_{rate} = 1.05 \times 10^{-4}$ mM s^{-1}), although a slightly lower V_{rate} was observed when compared with that of the free HRP ($V_{rate} = 1.28 \times 10^{-4}$ mM s^{-1}) at a given concentration (Figure 3c). However, the catalytic rate of the meso-MPN particles was higher than that of the HRP-loaded PCs (PCs/HRP; $V_{rate} = 7.14 \times 10^{-5}$ mM s^{-1}) and HRP-loaded mesoporous SiO_2 particles with a pore size of 50 nm (SiO_2 (50 nm)/HRP; $V_{rate} = 4.63 \times 10^{-5}$ mM s^{-1}; Figure S19).[44] The fast reaction kinetics displayed by the meso-MPN/HRP particles suggest a low diffusion barrier, likely due to the cubic network of large pore channels and high permeability originating from the MPNs.[23,45] Importantly, the meso-MPN/HRP particles could be effectively recycled at least 5 times with only a minimal decrease (~13%) in activity (Figure 3d), and no significant changes in the UV–vis spectra (Figure S15). In contrast, the mesoporous SiO_2 (50 nm)/HRP and PCs/HRP demonstrated enzymatic activity losses of 30% and 70%, respectively. These results indicate that the meso-MPN particles can effectively serve as high loading carriers for the immobilization and recyclability of enzymes.

CONCLUSION

In summary, we developed a strategy to construct ordered meso-MPN particles with a bicontinuous cubic network (40 nm) using PCs as templates and MPNs as the replica material. We observed a structured replica transitioning from PCs with double networks ($Im\bar{3}m$) to meso-MPN particles with single networks ($Pm\bar{3}m$). Proteins of different size, shape, and composition were loaded at high amounts (~360—485 mg g^{-1}) into the meso-MPN particles. The enzyme-loaded meso-MPN particles exhibited excellent catalytic activity (82% of the free enzyme) with recyclability (loss of ~13% activity over 5 cycles), which are attributed to the multifaceted nature of the MPN and bicontinuous ordered porosity. The judicious selection of metal ions and naturally abundant polyphenols with different functions (e.g., anticancer and neuroprotective effects) provide an opportunity for designing diverse meso-MPN particles using the current cubosome-enabled strategy for various applications.

EXPERIMENTAL SECTION

Synthesis of PS_{217}-*b*-PEO_{45} Block Copolymers. The PS_{217}-*b*-PEO_{45} block copolymer was synthesized by an atom transfer radical polymerization method that involved two steps (Figure S1).[46] The first step involved the synthesis of PEO-Br macroinitiator. Briefly, poly(ethylene glycol) methyl ether (average M_n ~2,000) (0.025 mol) was first dissolved in 200 mL of dichloromethane (DCM), followed by the addition of 10.1 mL of triethylamine (7.5 mmol). The resulting solution was cooled in an ice-water bath. Then, 6.2 mL of α-bromoisobutyryl bromide

(0.05 mol) in 20 mL of DCM solution was added dropwise under stirring. The reaction mixture was stirred for 12 h in an ice-water bath. A filter membrane was used to remove the triethylamine salt. The resulting solution was concentrated and precipitated in 500 mL of cold ether. The white precipitate was filtered, washed with cold ether three times, and dried under vacuum at room temperature overnight. In the second step, 2 g of PEO_{45}-Br, 133 mg of copper(I) bromide (0.93 mmol), and 206 μL of *N*,*N*,*N*′,*N*′,*N*″-pentamethyldiethylenetriamine (1 mmol) were introduced into a dried Schlenk flask. The flask was completely degassed with three freeze–pump–thaw cycles and refilled with N_2 in three cycles to remove oxygen. Then, a known amount of styrene was introduced into the flask via a syringe. The resulting mixture was further deoxygenated by three freeze–pump–thaw cycles. The flask was subsequently immersed in an oil bath at 110 °C under stirring to polymerize styrene. The reaction proceeded for 5 h before cooling to subzero temperatures by liquid nitrogen. The gel-like product was dissolved in 50 mL of THF and then filtered through basic alumina to remove copper complexes. The mixture solution then was concentrated and added dropwise to 500 mL of methanol. The resulting white precipitate was filtered and washed with methanol three times. The final product was dried under vacuum at room temperature overnight.

Self-Assembly of PS_{217}-*b*-PEO_{45} Block Copolymers in Solution. Polymer cubosomes with the double primitive cubic network were self-assembled by a simple cosolvent method. Typically, PS_{217}-*b*-PEO_{45} was dissolved in 2 mL of dioxane/dimethylformamide (v/v 92:8) mixture solution (1 wt%). The solution was stirred for 4 h at room temperature for complete dissolution of the copolymer. Water (50 wt%) was added at a controlled rate (1 mL h^{-1}) to the organic solution of block copolymers with stirring. The formed assemblies were collected by rapidly adding a 10-fold amount of water. The cubosomes were then purified by centrifugation (3000 *g*, 1 min) and washed with water to remove residual organic solvent.

Synthesis of Meso-MPN Particles. Typically, aliquots (1 mL) of EGCG (30 mM) and $FeCl_3.6H_2O$ (30 mM) solution were sequentially added to 20 mL of the cubosome aqueous solution (0.05% w/v). The suspension was vigorously stirred for 2 h to ensure complete diffusion of the polyphenol and metal ions into the cubosomes. The pH of the suspension was then raised by adding 25 mL of 3-(*N*-morpholino)propanesulfonic acid (MOPS) buffer (100 mM, pH 6.5) solution. The reaction was stirred for another 10 min. Unreacted supernatant was removed by centrifugation (3000 *g*, 1 min) and washing with Milli-Q water for three times. Dissolution of the polymer cubosomes was accomplished by washing the pellets with THF three times (3000 *g*, 1 min). The suspension was incubated with THF for 30 min under constant shaking (1000 rpm). The obtained ordered meso-MPN particles were washed with Milli-Q water twice (3000 *g*, 1 min) and resuspended in 20 mM MOPS (pH 7.4). The meso-MPN particle dispersion was stored at 4 °C for future use and used within 1 week of preparation.

Disassembly Experiments. The disassembly of the meso-MPN particles was studied by monitoring the release behavior of iron. Typically, an aliquot of the meso-MPN particles was dispersed in 20 mM MOPS (pH 7.4), 20 mM sodium acetate (pH 5.0), or 20 mM sodium acetate (pH 4.0) and incubated in a shaker bath at 37 °C for the desired time. The suspension was then centrifuged (3000 *g*, 2 min) to collect the supernatant. The iron concentration in the supernatant was determined by inductively coupled plasma optical emission spectrometry. The initial iron concentration of the meso-MPN particles was determined by incubating the meso-MPN particles in 1 M HCl overnight. The complete disassembly of the meso-MPN particles in 1 M HCl was confirmed from the resulting transparent suspension obtained and electron microscopy images.

Protein Loading Inside Different Carriers. Different carriers (5 mg), including meso-MPN particles, PCs, or SiO_2 with an average pore size of 8, 20, or 50 nm, were incubated with 5 mL of protein stock solution (1 mg mL^{-1}) in 50 mM phosphate buffer (pH 6.0) for 5 h. The protein-loaded carriers were washed three times with 50 mM phosphate buffer (pH 6.0). The amount of protein loaded inside the particles was determined by UV–vis spectroscopy by comparing the absorbance of the protein solution before loading with the supernatant after loading. The wavelength used to determine the loading amount of BHb, HRP, IgG, and GOx was 280 nm.

Catalytic Activity Test. The activity of the loaded HRP was evaluated according to the manufacturer's specifications. Briefly, free HRP, meso-MPN/HRP, PCs/HRP, or SiO_2/HRP particles were mixed with 50 mM phosphate-buffered saline (PBS) solution (pH 7.4) containing 25 μM amplex red and 0.5 mM hydrogen peroxide. Changes in the absorbance of the red oxidation product (resorufin) at 560 nm were monitored by UV–vis spectroscopy. The reaction rate of HRP was calculated from the extinction coefficient of resorufin (58,000 cm^{-1} M^{-1}). The catalysis rate was calculated from the first 100 s.

Recycling experiments were performed under the same condition as described above. After one cycle, particles were retrieved by centrifugation (3000 *g*, 2 min), washed with PBS, and reused in the subsequent cycle.

ASSOCIATED CONTENT

Supporting Information. Additional experimental procedures and characterization of the block copolymer, different metal ions and polyphenol-based meso-MPN particles, cargos loaded inside the meso-MPN particles, and SiO_2 with different pore sizes (PDF). This material is available free of charge via the Internet at http://pubs.acs.org.

AUTHOR INFORMATION

Corresponding Author

* fcaruso@unimelb.edu.au

Author Contributions

The manuscript was written through contributions of all authors.

Notes

The authors declare no competing financial interests.

ACKNOWLEDGMENT

This research was conducted and funded by the Australian Research Council (ARC) Centre of Excellence in Convergent Bio-Nano Science and Technology (project number CE140100036) and an ARC Discovery Project (DP170103331). F.C. acknowledges the award of a National Health and Medical Research Council Senior Principal Research Fellowship (GNT1135806). This work was performed in part at the Materials Characterisation and Fabrication Platform and the Bio21 Advanced Microscopy Facility at The University of Melbourne, and the Victorian Node of the Australian

National Fabrication Facility. We acknowledge Dr. Alex Duan for XPS measurements. Part of this research was conducted at the SAXS/WAXS beamline at the Australian Synchrotron, part of ANSTO. The authors acknowledge Yingjie Hu, Jingqu Chen, Yijiao Qu, Jiaying Song, and Dr. René Lafleur for helpful discussions.

REFERENCES

(1) Valtchev, V.; Tosheva, L. Porous Nanosized Particles: Preparation, Properties, and Applications. *Chem. Rev.* **2013**, *113*, 6734–6760.

(2) Wu, D.; Xu, F.; Sun, B.; Fu, R.; He, H.; Matyjaszewski, K. Design and Preparation of Porous Polymers. *Chem. Rev.* **2012**, *112*, 3959–4015.

(3) Wang, J.; Ma, Q.; Wang, Y.; Li, Z.; Li, Z.; Yuan, Q. New Insights into the Structure–Performance Relationships of Mesoporous Materials in Analytical Science. *Chem. Soc. Rev.* **2018**, *47*, 8766–8803.

(4) Krishna, R. Diffusion in Porous Crystalline Materials. *Chem. Soc. Rev.* **2012**, *41*, 3099–3118.

(5) Davis, M. E. Ordered Porous Materials for Emerging Applications. *Nature* **2002**, *417*, 813–821.

(6) Deng, Y.; Wei, J.; Sun, Z.; Zhao, D. Large-Pore Ordered Mesoporous Materials Templated from Non-Pluronic Amphiphilic Block Copolymers. *Chem. Soc. Rev.* **2013**, *42*, 4054–4070.

(7) Peng, L.; Hung, C. T.; Wang, S.; Zhang, X.; Zhu, X.; Zhao, Z.; Wang, C.; Tang, Y.; Li, W.; Zhao, D. Versatile Nanoemulsion Assembly Approach to Synthesize Functional Mesoporous Carbon Nanospheres with Tunable Pore Sizes and Architectures. *J. Am. Chem. Soc.* **2019**, *141*, 7073–7080.

(8) Spokoyny, A. M.; Kim, D.; Sumrein, A.; Mirkin, C. A. Infinite Coordination Polymer Nano- and Microparticle Structures. *Chem. Soc. Rev.* **2009**, *38*, 1218–1227.

(9) Kirchon, A.; Feng, L.; Drake, H. F.; Joseph, E. A.; Zhou, H. C. From Fundamentals to Applications: A Toolbox for Robust and Multifunctional MOF Materials. *Chem. Soc. Rev.* **2018**, *47*, 8611–8638.

(10) Deng, H.; Grunder, S.; Cordova, K. E.; Valente, C.; Furukawa, H.; Hmadeh, M.; Gándara, F.; Whalley, A. C.; Liu, Z.; Asahina, S.; Kazumori, H.; O'Keeffe, M.; Terasaki, O.; Stoddart, J. F.; Yaghi, O. M. Large-Pore Apertures in a Series of Metal-Organic Frameworks. *Science* **2012**, *336*, 1018–1023.

(11) Yaghi, O. M.; O'Keeffe, M.; Ockwig, N. W.; Chae, H. K.; Eddaoudi, M.; Kim, J. Reticular Synthesis and the Design of New Materials. *Science* **2003**, *423*, 705–714.

(12) Guillerm, V.; Xu, H.; Albalad, J.; Imaz, I.; Maspoch, D. Postsynthetic Selective Ligand Cleavage by Solid–Gas Phase Ozonolysis Fuses Micropores into Mesopores in Metal–Organic Frameworks. *J. Am. Chem. Soc.* **2018**, *140*, 15022–15030.

(13) Sun, L. B.; Li, J. R.; Park, J.; Zhou, H. C. Cooperative Template-Directed Assembly of Mesoporous Metal–Organic Frameworks. *J. Am. Chem. Soc.* **2012**, *134*, 126–129.

(14) Bradshaw, D.; El-Hankari, S.; Lupica-Spagnolo, L. Supramolecular Templating of Hierarchically Porous Metal–Organic Frameworks. *Chem. Soc. Rev.* **2014**, *43*, 5431–5443.

(15) Guan, H. -Y.; LeBlanc, R. J.; Xie, S. -Y.; Yue, Y. Recent Progress in the Syntheses of Mesoporous Metal–Organic Framework Materials. *Coord. Chem. Rev.* **2018**, *369*, 76–90.

(16) Lin, Z.; Liu, S.; Mao, W.; Tian, H.; Wang, N.; Zhang, N.; Tian, F.; Han, L.; Feng, X.; Mai, Y. Tunable Self-Assembly of Diblock Copolymers into Colloidal Particles with Triply Periodic Minimal Surfaces. *Angew. Chem. Int. Ed.* **2017**, *56*, 7135–7140.

(17) La, Y.; Park, C.; Shin, T. J.; Joo, S. H.; Kang, S.; Kim, K. T. Colloidal Inverse Bicontinuous Cubic Membranes of Block Copolymers with Tunable Surface Functional Groups. *Nat. Chem.* **2014**, *6*, 534–541.

(18) Yu, H.; Qiu, X.; P. Nunes, S.; Peinemann, K. V. Colloidal Inverse Bicontinuous Cubic Membranes of Block Copolymers with Tunable Surface Functional Groups. *Nat. Commun.* **2014**, *5*, 4110.

(19) Groschel, A. H.; Walther, A. Block Copolymer Micelles with Inverted Morphologies. *Angew. Chem. Int. Ed.* **2017**, *56*, 10992–10994.

(20) Lyu, X.; Xiao, A.; Zhang, W.; Hou, P.; Gu, K.; Tang, Z.; Pan, H.; Wu, F.; Shen, Z.; Fan, X. H. Head–Tail Asymmetry as the Determining Factor in the Formation of Polymer Cubosomes or Hexasomes in a Rod–Coil Amphiphilic Block Copolymer. *Angew. Chem. Int. Ed.* **2018**, *57*, 10132–10136.

(21) Lv, F.; An, Z.; Wu, P. Scalable Preparation of Alternating Block Copolymer Particles with Inverse Bicontinuous Mesophases. *Nat. Commun.* **2019**, *10*, 1397.

(22) La, Y.; Song, J.; Jeong, M. G.; Cho, A.; Jin, S. M.; Lee, E.; Kim, K. T. Templated Synthesis of Cubic Crystalline Single Networks Having Large Open-Space Lattices by Polymer Cubosomes. *Nat. Commun.* **2018**, *9*, 5327.

(23) Ejima, H.; Richardson, J. J.; Liang, K.; Best, J. P.; van Koeverden, M. P.; Such, G. K.; Cui, J.; Caruso, F. One-Step Assembly of Coordination Complexes for Versatile Film and Particle Engineering. *Science* **2013**, *341*, 154–157.

(24) Guo, J.; Ping, Y.; Ejima, H.; Alt, K.; Meissner, M.; Richardson, J. J.; Yan, Y.; Peter, K.; von Elverfeldt, D.; Hagemeyer, C. E.; Caruso, F. Engineering Multifunctional Capsules through the Assembly of Metal–Phenolic Networks. *Angew. Chem. Int. Ed.* **2014**, *53*, 5546–5551.

(25) Rahim, M. A.; Kempe, K.; Müllner, M.; Ejima, H.; Ju, Y.; van Koeverden, M. P.; Suma, T.; Braunger, J. A.; Leeming, M. G.; Abrahams, B. F.; Caruso, F. Surface-Confined Amorphous Films from Metal-Coordinated Simple Phenolic Ligands. *Chem. Mater.* **2015**, *27*, 5825–5832.

(26) Guo, J.; Tardy, B. L.; Christofferson, A. J.; Dai, Y.; Richardson, J. J.; Zhu, W.; Hu, M.; Ju, Y.; Cui, J.; Dagastine, R. R.; Yarovsky, I.; Caruso, F. Modular Assembly of Superstructures from Polyphenol-Functionalized Building Blocks. *Nat. Nanotechnol.* **2016**, *11*, 1105–1111.

(27) Dai, Y.; Yang, Z.; Cheng, S.; Wang, Z.; Zhang, R.; Zhu, G.; Wang, Z.; Yung, B. C.; Tian, R.; Jacobson, O.; Xu, C.; Ni, Q.; Song, J.; Sun X.; Niu, G.; Chen, X. Toxic Reactive Oxygen Species Enhanced Synergistic Combination Therapy by Self-Assembled Metal-Phenolic Network Nanoparticles. *Adv. Mater.* **2018**, *30*, 1704877.

(28) Luo, W.; Xiao, G.; Tian, F.; Richardson, J. J.; Wang, Y.; Zhou, J.; Guo, J.; Liao, X.; Shi, B. Engineering Robust Metal–Phenolic Network Membranes for Uranium Extraction from Seawater. *Energy Environ. Sci.* **2019**, *12*, 607–614.

(29) Borgese, N.; Francolini, M.; Snapp, E. Endoplasmic Reticulum Architecture: Structures in Flux. *Curr. Opin. Cell Biol.* **2006**, *18*, 358–364.

(30) Han, L.; Che, S. An Overview of Materials with Triply Periodic Minimal Surfaces and Related Geometry: From Biological Structures to Self-Assembled Systems. *Adv. Mater.* **2018**, *30*, 1705708.

(31) Barriga, H. M. G.; Holme, M. N.; Stevens, M. M. Cubosomes: The Next Generation of Smart Lipid Nanoparticles? *Angew. Chem. Int. Ed.* **2019**, *58*, 2958–2978.

(32) Demurtas, D.; Guichard, P.; Martiel, I.; Mezzenga, R.; Hébert, C.; Sagalowicz, L. Direct Visualization of Dispersed Lipid Bicontinuous Cubic Phases by Cryo-Electron Tomography. *Nat. Commun.* **2015**, *6*, 8915.

(33) Tanaka, S.; Maki, S.; Ataka, M. Structural Transitions of the Mono-Olein Bicontinuous Cubic Phase Induced by Inclusion of Protein Lysozyme Solutions. *Phys. Rev. E* **2006**, *73*, 061510.

(34) Akbar, S.; Elliott, J. M.; Rittman, M.; Squires, A. M. Facile Production of Ordered 3D Platinum Nanowire Networks with "Single Diamond" Bicontinuous Cubic Morphology. *Adv. Mater.* **2013**, *25*, 1160–1164.

(35) Takatsu, H.; Hernandez, O.; Yoshimune, W.; Prestipino, C.; Yamamoto, T.; Tassel, C.; Kobayashi, Y.; Batuk, D.; Shibata, Y.; Abakumov, A. M.; Brown, C. M.; Kageyama, H. Cubic Lead Perovskite $PbMoO_3$ with Anomalous Metallic Behavior. *Phys. Rev. B* **2017**, *95*, 155105.

(36) Mao, W.; Cao, X.; Sheng, Q.; Han, L.; Che, S. Silica Scaffold with Shifted "Plumber's Nightmare" Networks and Their Interconversion into Diamond Networks. *Angew. Chem. Int. Ed.* **2017**, *56*, 10670–10675.

(37) Rahim, M. A.; Bjornmalm, M.; Bertleff-Zieschang, N.; Besford, Q.; Mettu, S.; Suma, T.; Faria, M.; Caruso, F. Rust-Mediated Continuous Assembly of Metal–Phenolic Networks. *Adv. Mater.* **2017**, *29*, 1606717.

(38) Ma, Y.; Björnmalm, M.; Wise, A. K.; Cortez-Jugo, C.; Revalor, E.; Ju, Y.; Feeney, O. M.; Richardson, R. T.; Hanssen, E.; Shepherd, R. K.; Porter, C. J. H.; Caruso, F. Gel-Mediated Electrospray Assembly of Silica Supraparticles for Sustained Drug Delivery. *ACS Appl. Mater. Interfaces* **2018**, *10*, 31019–31031.

(39) Rahim, M. A.; Kristufek, S. L.; Pan, S.; Richardson, J. J.; Caruso, F. Phenolic Building Blocks for the Assembly of Functional Materials. *Angew. Chem. Int. Ed.* **2019**, *58*, 1904–1927.

(40) Quideau, S.; Deffieux, D.; Douat-Casassus, C.; Pouysegu, L. Plant Polyphenols: Chemical Properties, Biological Activities, and Synthesis. *Angew. Chem. Int. Ed.* **2011**, *50*, 586–621.

(41) Lee, H.; Dellatore, S. M.; Miller, W. M.; Messersmith, P. B. Mussel-Inspired Surface Chemistry for Multifunctional Coatings. *Science* **2007**, *318*, 426–430.

(42) Liu, J.; Guo, Zi.; Liang, K. Biocatalytic Metal-Organic Framework-Based Artificial Cells. *Adv. Funct. Mater.* **2019**, *29*, 1905321.

(43) Watkins, D. W.; Jenkins, J. M. X.; Grayson, K. J.; Wood, N.; Steventon, J. W.; Le Vay, K. K.; Goodwin, M. I.; Mullen, A. S.; Bailey, H. J.; Crump, M. P.; MacMillan, F.; Mulholland, A. J.; Cameron, G.; Sessions, R. B.; Mann, S.; Anderson, J. L. R. Construction and In Vivo Assembly of a Catalytically Proficient and Hyperthermostable De Novo Enzyme. *Nat. Commun.* **2017**, *8*, 358.

(44) Jaladi, H.; Katiyar, A.; Thiel, S. W.; Guliants, V. V.; Pinto, N. G. Effect of Pore Diffusional Resistance on Biocatalytic Activity of *Burkholderia Cepacia* Lipase Immobilized on SBA-15 Hosts. *Chem. Eng. Sci.* **2009**, *64*, 1474–1479.

(45) Shen, K.; Zhang, L.; Chen, X.; Liu, L.; Zhang, D.; Han, Y.; Chen, J.; Long, J.; Luque, R.; Li, Y.; Chen, B. Ordered Macro-Microporous Metal-Organic Framework Single Crystals. *Science* **2018**, *359*, 206–210.

(46) Deng, Y.; Yu, T.; Wan, Y.; Shi, Y.; Meng, Y.; Gu, D.; Zhang, L.; Huang, Y.; Liu, C.; Wu, X.; Zhao, D. Ordered Mesoporous Silicas and Carbons with Large Accessible Pores Templated from Amphiphilic Diblock Copolymer Poly (Ethylene Oxide)-*b*-Polystyrene. *J. Am. Chem. Soc.* **2007**, *129*, 1690–1697.

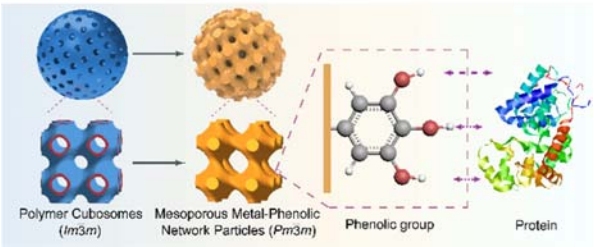
Polymer Cubosomes
(Im3m)
Mesoporous Metal-Phenolic
Network Particles (Pm3m)
Phenolic group
Protein